

# Cross-section measurement of $(n,2n)$ reactions for Nd isotopes induced by 14 MeV neutrons

Qiang Wang<sup>1,2</sup> · Bing-Jun Chen<sup>1</sup> · Qian Zhang<sup>1</sup> · Si-Min Cai<sup>1</sup> · Chang-Lin Lan<sup>1,2</sup> · Kai-Hong Fang<sup>1,2</sup>

Received: 21 May 2018/Revised: 7 September 2018/Accepted: 13 September 2018/Published online: 2 January 2019  
© China Science Publishing & Media Ltd. (Science Press), Shanghai Institute of Applied Physics, the Chinese Academy of Sciences, Chinese Nuclear Society and Springer Nature Singapore Pte Ltd. 2019

**Abstract** Cross-sections of the  $(n,2n)$  reactions for neodymium (Nd) isotopes induced by 14 MeV neutrons were measured in this work by using the activation and relative methods. The measured cross-sections of the  $^{150}\text{Nd}(n,2n)^{149}\text{Nd}$ ,  $^{148}\text{Nd}(n,2n)^{147}\text{Nd}$ , and  $^{142}\text{Nd}(n,2n)^{141}\text{Nd}$  reactions were  $1854 \pm 81$ ,  $1789 \pm 119$ , and  $1559 \pm 98$  mb, respectively, at a neutron energy of  $14.2 \pm 0.2$  MeV, and  $1485 \pm 74$ ,  $1726 \pm 85$ , and  $1670 \pm 119$  mb, respectively, at  $14.9 \pm 0.2$  MeV. The results were compared with the experimental values from the reported literature, with the evaluated data from the ENDF/B-VII.1, CENDL-3.1, and JENDL-4.0 libraries, and with the curves calculated by the Talys-1.8 code.

**Keywords** Cross-section · Neodymium ·  $(n,2n)$  reaction · Activation method · 14 MeV neutron

## 1 Introduction

Cross-section is one of the most important measurable quantities in atomic, nuclear, and particle physics. Neutron cross-section plays a key role in nuclear transmutation, nuclear reactions, radiation damage, and other such phenomena [1–6]. In the field of nuclear science, it is therefore

very important to make an accurate measurement of the cross-section and excitation-function induced by neutrons [7].

Neodymium (Nd) is a rare-earth element that can be widely applied to fission reactors. The cross-sections of the  $(n,2n)$  reactions for Nd isotopes induced by 14 MeV neutrons are vital for establishing fission product poison in fast reactors and are therefore reliable burn up monitors for fast reactor fuels [8]. Most of the measurements for cross-sections of the  $(n,2n)$  reactions for Nd isotopes were taken last century [9–24], *e.g.*, Wille and Fink [9], Bari [14], Qaimin [15], and Gmuca and Ribansky [17]. In the twenty-first century, two main experimental results for Nd were reported by Pu et al. [25] and by Luo et al. [26]. However, the experimental results are not in good agreement with each other. As many factors affect the accuracy of the experimental results, *e.g.*, different experimental methods, different experimental technologies, and different parameters and monitor reactions, it is valuable to re-measure the cross-sections of the neodymium isotopes.

Our group has been engaged in the measurement of nuclear data for many years [27–32]. In the present study,  $(n,2n)$  reaction cross-sections for  $^{150}\text{Nd}$ ,  $^{148}\text{Nd}$  and  $^{142}\text{Nd}$  neodymium isotopes were measured at 14.2 and 14.9 MeV energy points with a high-resolution gamma ray detector by using an activation technique and  $^{27}\text{Al}(n,\alpha)^{24}\text{Na}$  as a monitor reaction. The deduced cross-sections of the  $^{150}\text{Nd}(n,2n)^{149}\text{Nd}$ ,  $^{148}\text{Nd}(n,2n)^{147}\text{Nd}$  and  $^{142}\text{Nd}(n,2n)^{141}\text{Nd}$  reactions were compared with literature results, with evaluated data from libraries, and with theoretical values calculated by the Talys-1.8 code.

✉ Kai-Hong Fang  
fangkh@lzu.edu.cn

<sup>1</sup> School of Nuclear Science and Technology, Lanzhou University, Lanzhou 730000, China

<sup>2</sup> Engineering Research Center for Neutron Application Technology, Ministry of Education, Lanzhou University, Lanzhou 730000, China

## 2 Experimental details

### 2.1 Samples and irradiations

Neodymium oxide powder (purity: 99.95%) was pressed at  $10 \text{ t/cm}^2$  into disk samples (diameter:  $\sim 12.7 \text{ mm}$ , thickness:  $\sim 1.6 \text{ mm}$ ). Two such disks were prepared. The masses of the samples were 1.7 and 1.6 g. Monitor foils of aluminum (Al) (purity: 99.9%, thickness:  $50 \mu\text{m}$ ) and standard niobium (Nb) and zirconium (Zr) (purity: 99.99%, thickness:  $0.5 \text{ mm}$ ) with the same size as the Nd sample disk were placed on the front and back surfaces of each sample, which was covered by a polyethylene bag. A cadmium (Cd) foil was covered the sandwiched sample to capture the scattered thermal neutrons during the irradiation.

The bombardment was performed at the 14 MeV neutron generator, OKTAVIAN, in the Division of Sustainable Energy and Environmental Engineering of Osaka University, Japan. In brief, an energetic deuteron beam with  $250 \mu\text{A}@265 \text{ keV}$  bombarded a T-Ti target to produce 14 MeV energy region neutrons via a  $\text{T}(d,n)^4\text{He}$  reaction. Since the absolute value of neutron flux can be eliminated by neutron activation analysis, the essential factor is the neutron fluctuation, which was monitored during the entire bombardment process. The intensity of the neutron source can be gauged by its neutron yield, which was estimated to be  $1.5 \times 10^{11}$  neutrons/s by the monitor reaction  $^{27}\text{Al}(n,\alpha)^{24}\text{Na}$ .

The two samples were mounted at angles of  $45^\circ$  and  $85^\circ$  relative to the direction of the deuteron beam, at a distance of 3.5 cm from the T-Ti target. The sample positions are shown in Fig. 1.

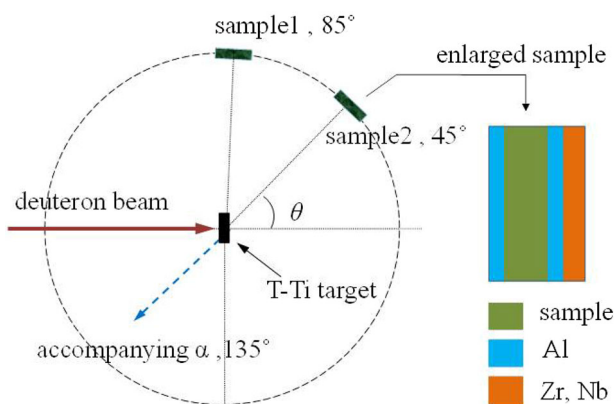


**Fig. 1** The sample assembly and its position with the T-Ti target (Color online)

### 2.2 Neutron energy

Neutron energy was calibrated via the method of cross-section ratio, *i.e.*,  $^{90}\text{Zr}(n,2n)^{89}\text{Zr}$  to  $^{93}\text{Nb}(n,2n)^{92\text{m}}\text{Nb}$  [33] and was also estimated by the following formula, which is deduced from the  $Q$ -equation of the nuclear reaction:

$$E_n = \left\{ 0.28E_d^{0.5} \cos\theta + [(0.4 + 0.08\cos^2\theta)E_d + 0.8Q]^{0.5} \right\}^2, \quad (1)$$

where  $E_d$  is the deuteron energy (in MeV),  $E_n$  is the neutron energy (in MeV) at detection angle  $\theta$ , and the  $Q$  value is equal to 17.6 MeV. The uncertainty in the neutron energy, estimated to be 0.2 MeV, arises from the diameter of the beam ( $\sim 20 \text{ mm}$ ) and sample (12.7 mm), the cross-section ratio of  $^{90}\text{Zr}(n,2n)^{89}\text{Zr}$  to  $^{93}\text{Nb}(n,2n)^{92\text{m}}\text{Nb}$  reactions, and the energy loss of deuterons in the thick T-Ti target.

### 2.3 Measurement of radioactivity

The samples were irradiated for  $\sim 8 \text{ h}$  and then cooled for  $\sim 50 \text{ min}$  to 10 h before starting the activity measurement. The gamma activities of  $^{149}\text{Nd}$ ,  $^{147}\text{Nd}$  and  $^{141}\text{Nd}$  were detected by a low-background HPGe gamma ray spectrometer (ORTEC, GMX30P4) that has a relative efficiency of  $\sim 68\%$ . The detection efficiency of the spectrometer was calibrated using the standard sources  $^{60}\text{Co}$ ,  $^{137}\text{Cs}$ ,  $^{152}\text{Eu}$ , and  $^{241}\text{Am}$ . The detection efficiency  $\varepsilon$  satisfied the linear relationship  $\ln\varepsilon = a + b\ln E_\gamma$  [34, 35] with gamma ray energy  $E_\gamma$ . The abundance of the target isotope and its decay data are shown in Table 1 [36].

### 2.4 Calculation of cross-sections

The theoretical formula for measuring the cross-section using the relative method is given as [27, 28, 37]

$$\sigma_x = \frac{[\varepsilon I_\gamma \eta \text{KSMD}]_0 [\lambda \text{AFC}]_x}{[\varepsilon I_\gamma \eta \text{KSMD}]_x [\lambda \text{AFC}]_0} \sigma_0, \quad (2)$$

where terms with subscript 0 were set as the parameters of the monitoring reaction, and terms with subscript  $x$  were set as the parameters of reactions to be tested.

In this formula,  $\varepsilon$  is the detection efficiency;  $I_\gamma$  is the branching ratio of the characteristic gamma ray;  $\eta$  is the isotopic abundance of the activated nuclide;  $S$  is a growth factor of the product nuclide, *i.e.*,  $S = 1 - e^{-\lambda T}$  where  $T$  is the total irradiation time and  $\lambda$  is the decay constant;  $M$  is the sample mass;  $D = e^{-\lambda t_1} - e^{-\lambda t_2}$  represents a collection factor where  $t_1$  is the time interval from the end of irradiation to the beginning of the measurement and  $t_2$  is the time interval to the end of the measurement;  $A$  is the atomic

**Table 1** Some parameters related to all reactions

| Reactions                                | Isotopic abundance | Decay modes      | Product half-life $T_{1/2}$ | $\gamma$ -ray energy $E_\gamma$ (keV) | $\gamma$ -ray intensity $I_\gamma$ |
|--|--------------------|------------------|-----------------------------|---------------------------------------|------------------------------------|
| $^{150}\text{Nd}(n,2n)^{149}\text{Nd}$   | 5.64% 3            | $\beta^-$ (100%) | 1.728 h 1                   | 211.309 7                             | 25.9% 14 <sup>a</sup>              |
| $^{148}\text{Nd}(n,2n)^{147}\text{Nd}$   | 5.76% 3            | $\beta^-$ (100%) | 10.98 d 1                   | 531.016 22                            | 13.4% 3                            |
| $^{142}\text{Nd}(n,2n)^{141}\text{Nd}$   | 27.13% 12          | EC (100%)        | 2.49 h 3                    | 1126.91 20                            | 0.80% 3                            |
| $^{27}\text{Al}(n,\alpha)^{24}\text{Na}$ | 100%               | $\beta^-$ (100%) | 14.997 h 12                 | 1368.626 5                            | 99.9936% 15                        |

<sup>a</sup>This value is taken from NNDC

weight of the activated nuclide; and  $C$  is the net count of the particular gamma ray.

$F$  is a correction factor, expressed as

$$F = f_c \times f_g \times f_s, \tag{3}$$

where the three parts ( $f_c$ ,  $f_g$ , and  $f_s$ ), correspond to coincidence summing, counting geometry, and self-absorption, respectively [38].

$K$  is the so-called neutron flux fluctuation correction factor, which is expressed as

$$K = \frac{\sum_i^L \Phi_i (1 - e^{-\lambda \Delta t_i}) e^{-\lambda T_i}}{\Phi S}, \tag{4}$$

where  $L$  is the segment number of the divided radiation time interval;  $\Delta t_i$  is the time interval for each segment;  $T_i$  is the interval from the end of the  $i$ th segment to the end of bombardment; and  $\Phi_i$  and  $\Phi$  are the averaged neutron fluxes during  $\Delta t_i$  and  $T$ , respectively.

The uncertainties in this work originate mainly from isotopic abundance, weight of samples, cross-section of the monitor reaction, branching ratio of gamma ray, half-life of the particular nuclide, detector efficiency, self-absorption correction, counting geometry, and counting statistics, as shown in Table 2.

**Table 2** The uncertainty sources and their estimated values

| Source of uncertainty  | Uncertainty (%) |
|------------------------|-----------------|
| Isotopic abundance     | ~ 0.5           |
| Weight of samples      | 0.1             |
| Standard cross-section | ~ 2             |
| Branching ratio        | 0.15–5.4        |
| Half-life              | 0.06–1.2        |
| Detector efficiency    | 2.0–2.5         |
| Self-absorption        | ~ 0.5           |
| Counting geometry      | 1.5             |
| Measuring time         | ~ 0.1           |
| Counting statistics    | 0.35–5          |

### 3 Results and discussion

#### 3.1 Experimental results

To focus clearly on the product nuclide of interest when collecting the gamma spectrum, different time parameters were applied that were based on the half-life of particular product. For example, times of ~ 1 h for cooling and ~ 8 h for measuring were used for  $^{149}\text{Nd}$  and  $^{141}\text{Nd}$ ; meanwhile, times of ~ 16 h for cooling and ~ 9 h for measuring were used for  $^{147}\text{Nd}$ .

Figure 2 illustrates a typical gamma ray spectrum accumulated by the activated  $\text{Nd}_2\text{O}_3$  sample, which was measured for 8 h after a cooling time of 1 h from the end of irradiation. In Fig. 2, (a) is a full gamma ray spectrum with the characteristic peaks of interest of  $^{141}\text{Nd}$  and  $^{24}\text{Na}$ , (b) is a partial gamma ray spectrum at low energy with the peaks of  $^{147}\text{Nd}$  and  $^{149}\text{Nd}$ , and (c) is the background spectrum with the gamma rays of  $^{40}\text{K}$ , which came from the lead chamber. This background was measured for ~ 8 h with the  $\text{Nd}_2\text{O}_3$  sample before irradiation in the chamber.

Four characteristic gamma peaks were marked for the  $^{141}\text{Nd}$  and  $^{147}\text{Nd}$  products, and more than ten characteristic

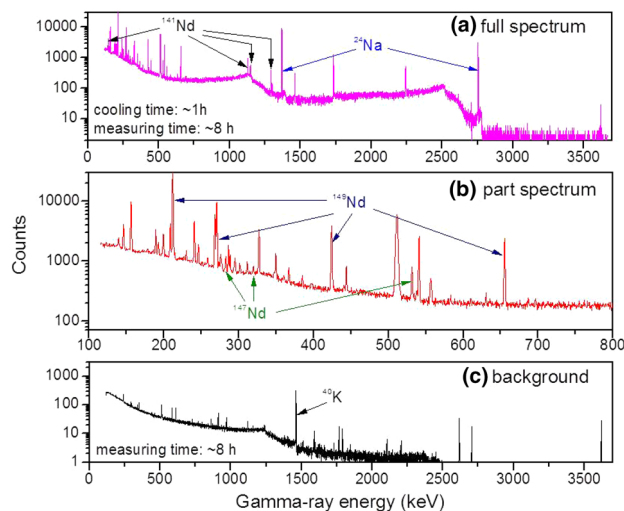


**Fig. 2** Gamma ray spectra (the x-axis is the gamma ray energy in keV; the y-axis is the counts per channel) (Color online)

gamma peaks were clearly seen for  $^{149}\text{Nd}$ . We chose the common characteristic peaks with the larger branch to deduce the cross-sections. Following the activation formula in Eq. (2), the cross-sections of the three  $(n,2n)$  reactions were deduced. In the calculation, the cross-section of the monitor reaction was obtained by fitting the evaluated data from ENDF/B-VII.1 [39]. The deduced cross-sections are summarized in Table 3.

### 3.2 Discussion

The evaluated data from databases (of ENDF/B-VII.1 [39], CENDL-3.1 [40] and JENDL-4.0 [41]) were used to show the trend of  $(n,2n)$  reaction cross-sections for Nd isotopes in the energy region of  $E_n < 20$  MeV. Moreover, the results obtained in this work were compared with literature data and with values calculated by the Talys-1.8 code.

The deduced cross-sections are plotted in Figs. 3, 4 and 5 together with the previous measurements. To facilitate comparison, the values calculated by the Talys-1.8 program and the evaluated data of the above-mentioned databases [39–41] are plotted in the same figures. Figures 3, 4 and 5 show that the cross-sections increase as neutron energy increases from the threshold, *i.e.*, 7.4 MeV for  $^{148}\text{Nd}(n,2n)^{147}\text{Nd}$ , 7.3 MeV for  $^{148}\text{Nd}(n,2n)^{147}\text{Nd}$ , and 9.8 MeV for the  $^{142}\text{Nd}(n,2n)^{141}\text{Nd}$  reaction. The increasing trend gradually reaches a maximum value and then decreases with neutron energy. Most of the experimental data are concentrated in the neutron energy region of 13–15 MeV, while a few experimental results are in a broad neutron energy region, *e.g.*, those of Frehaut et al. [19] in the three reactions, Bormann et al. [23] in the  $^{142}\text{Nd}(n,2n)^{141}\text{Nd}$  reaction, and Do et al. [18] in the  $^{150}\text{Nd}(n,2n)^{149}\text{Nd}$  reaction.

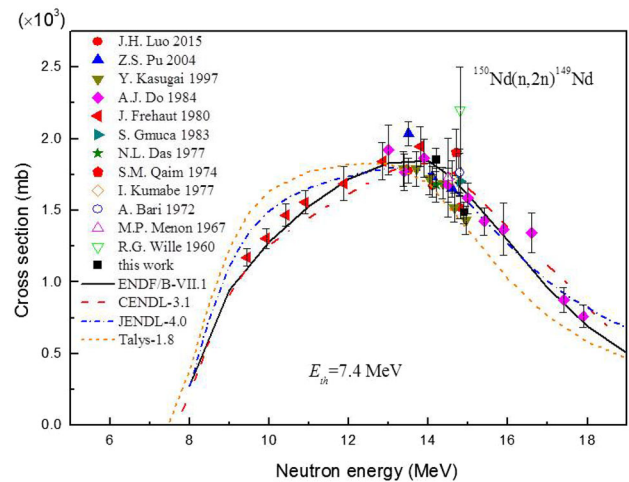
#### (a) $^{150}\text{Nd}(n,2n)^{149}\text{Nd}$ reaction

Figure 3 shows the deduced cross-sections, as well as the evaluated data from the databases [39–41], for the

**Table 3** The  $(n,2n)$  reaction cross-sections for Nd isotopes<sup>a</sup>

| Reactions                                | Cross-sections (in mb) |                |
|--|------------------------|----------------|
|  | 14.2 ± 0.2 MeV         | 14.9 ± 0.2 MeV |
| $^{150}\text{Nd}(n,2n)^{149}\text{Nd}$   | 1854 ± 81              | 1485 ± 74      |
| $^{148}\text{Nd}(n,2n)^{147}\text{Nd}$   | 1789 ± 119             | 1726 ± 85      |
| $^{142}\text{Nd}(n,2n)^{141}\text{Nd}$   | 1559 ± 98              | 1670 ± 119     |
| $^{27}\text{Al}(n,\alpha)^{24}\text{Na}$ | 119.8 ± 2.4            | 111.6 ± 2.2    |

<sup>a</sup>Errors quoted in the cross-section data arise from the uncertainties of weight of samples, detector efficiency, self-absorption of gamma ray, counting geometry, measuring times and counting statistics



**Fig. 3** The cross-sections of the  $^{150}\text{Nd}(n,2n)^{149}\text{Nd}$  reaction (Color online)

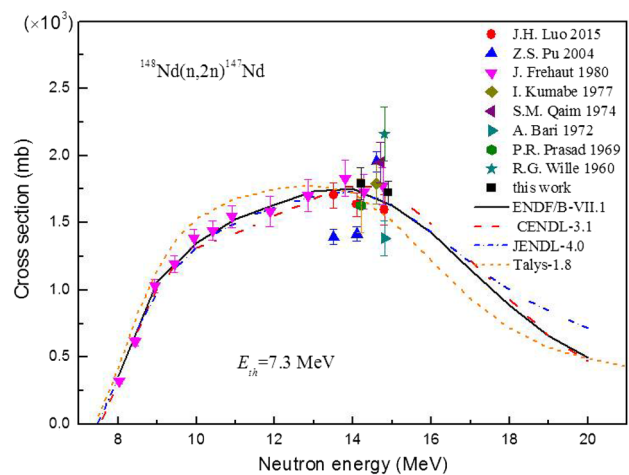


**Fig. 4** The cross-sections of the  $^{148}\text{Nd}(n,2n)^{147}\text{Nd}$  reaction (Color online)

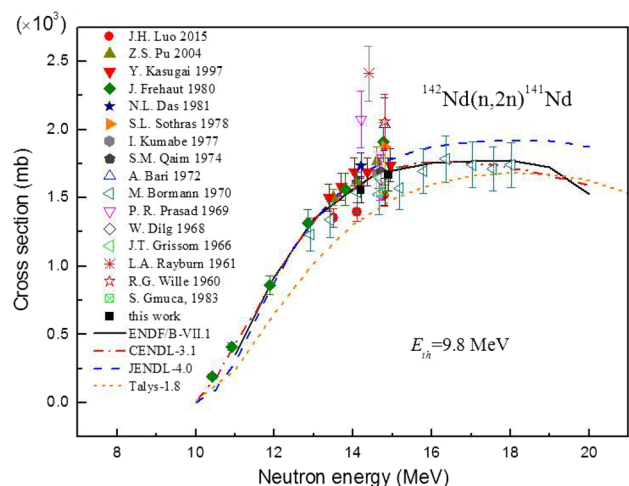


**Fig. 5** The cross-sections of the  $^{142}\text{Nd}(n,2n)^{141}\text{Nd}$  reaction (Color online)

$^{150}\text{Nd}(n,2n)^{149}\text{Nd}$  reaction. Ten measurements (Wille and Fink [9], Menon and Cuypers [21], Bari [14], Das et al. [20], Kumabe et al. [24], Gmuca and Ribansky [17], Kasugai et al. [22], Pu et al. [25], and Luo et al. [26]) were in the neutron energy region of 13–15 MeV, while two groups measured the cross-section in a broad energy region (Frehaut et al. [19] in 9–14 MeV, and Do et al. [18] in 12–18 MeV).

The present results are consistent with literature data within the uncertainty except with those of Wille and Fink [9]. In that study, a single value was obtained at 14.8 MeV that is approximately 30% higher than those of other groups. In the 9–18 MeV energy region, the excitation curves of the evaluated data from recent studies [39–41] are similar to the measured results of Do et al. [18], Kasugai et al. [22], Frehaut et al. [19], Pu et al. [25], and Luo et al. [26]. The calculated results from the Talys-1.8 code have the same trend but are lower than others in the 13–15 MeV energy region. The present results are consistent with others but have a slightly decreasing trend.

(b)  $^{148}\text{Nd}(n,2n)^{147}\text{Nd}$  reaction

A few groups have investigated the cross-section of the  $^{148}\text{Nd}(n,2n)^{147}\text{Nd}$  reaction previously (Wille and Fink [9], Prasad et al. [13], Bari [14], Qaim [15], Kumabe et al. [24], Frehaut et al. [19], Pu et al. [25], and Luo et al. [26]), and those values are all plotted in Fig. 4. Our experimental results are in agreement with the values given by Kumabe et al. [24] and Frehaut et al. [19], and also consistent with the results of the databases [39–41] and the Talys-1.8 code in the 13.8–15.0 MeV energy region. The experimental data reported by Luo et al. [26] and Prasad et al. [13] are slightly lower than ours, but the results of Qaim [15] are higher. The results of Wille and Fink [9], Bari [14], and Pu et al. [25] deviate greatly.

(c)  $^{142}\text{Nd}(n,2n)^{141}\text{Nd}$  reaction

Figure 5 shows the cross-sections of the  $^{142}\text{Nd}(n,2n)^{141}\text{Nd}$  reaction. In general, the results from the present work are consistent with the reported data from Grissom et al. [11], Dilg et al. [12], Qaim [15], Bormann et al. [23], and Kumabe et al. [24] and with the evaluated data of the databases [39, 40]. These values are slightly lower than the results of Pu et al. [25], Das et al. [20], Sothras and Salaita [16], Kasugai et al. [22] and the evaluated data from JENDL-4.0 [41], and slightly higher than those reported by Gmuca and Ribansky [17] and Luo et al. [26]. The results from Wille and Fink [9], Rayburn [10], and Prasad et al. [13] deviate greatly from the evaluated data. Values from Frehaut et al. [19], Bormann et al. [23] and Luo et al. [26] have a trend similar to that of the evaluated cross-section curves [39–41]. The calculated values are lower than other data in the  $E_n < 20$  MeV energy region.

## 4 Conclusion

Cross-sections of the  $^{150}\text{Nd}(n,2n)^{149}\text{Nd}$ ,  $^{148}\text{Nd}(n,2n)^{147}\text{Nd}$ , and  $^{142}\text{Nd}(n,2n)^{141}\text{Nd}$  reactions were measured at neutron energies of 14.2 and 14.9 MeV. An optimized schedule of cooling and measuring was arranged according to half-life to get a better gamma ray spectrum for the product isotope of interest. The measured cross-sections were compared with the reported results, with evaluated data from databases [39–41], and with theoretical results from the Talys-1.8 program. The present results are generally consistent with the evaluated data and with other literature data at 14.2 and 14.9 MeV neutron energies.

**Acknowledgements** The authors would like to thank Prof. Murata at Osaka University, Japan, for the excellent support during the measurements.

## References

1. E.T. Cheng, Radioactivity aspects of fusion reactors. *Fusion Eng. Des.* **10**, 231–242 (1989). [https://doi.org/10.1016/0920-3796\(89\)90058-6](https://doi.org/10.1016/0920-3796(89)90058-6)
2. X.J. Sun, C.H. Pan, G.G. Yu et al., Pre-neutron-emission mass distribution for reaction  $^{232}\text{Th}(n,f)$  up to 60 MeV. *Commun. Theor. Phys.* **62**, 711–716 (2014). <https://doi.org/10.1088/0253-6102/62/5/14>
3. W.A. Metwally, S. El-Sayed, A. Ababneh et al., Flux measurements for a DD neutron generator using neutron activation analysis. *Nucl. Sci. Tech.* **29**, 52 (2018). <https://doi.org/10.1007/s41365-018-0385-1>
4. Z.Q. Chen, Recent progress in nuclear data measurement for ADS at IMP. *Nucl. Sci. Tech.* **28**, 184 (2017). <https://doi.org/10.1007/s41365-017-0335-3>
5. S. Zhang, Y.B. Nie, J. Ren et al., Benchmarking of JEFF-3.2, FENDL-3.0 and TENDL-2014 evaluated data for tungsten with 14.8 MeV neutrons. *Nucl. Sci. Tech.* **28**, 27 (2017). <https://doi.org/10.1007/s41365-017-0192-0>
6. R. Ogul, N. Buyukcizmeci, A. Ergun et al., Production of neutron-rich exotic nuclei in projectile fragmentation at Fermi energies. *Nucl. Sci. Tech.* **28**, 18 (2017). <https://doi.org/10.1007/s41365-016-0175-6>
7. Y.D. Song, H.L. Wei, C.W. Ma et al., Improved FRACS parameterizations for cross sections of isotopes near the proton drip line in projectile fragmentation reactions. *Nucl. Sci. Tech.* **29**, 96 (2018). <https://doi.org/10.1007/s41365-018-0439-4>
8. R.A. Anderl, Y.D. Harker, F. Schmittroth, Neodymium, samarium and europium capture cross-section adjustments based on EBR-II integral measurements. No. CONF-791223-2. Idaho National Engineering Lab., Idaho Falls (USA); Hanford Engineering Development Lab., Richland, 1979
9. R.G. Wille, R.W. Fink, Activation cross-sections for 14.8 MeV neutrons and some new radioactive nuclides in the rare earth region. *Phys. Rev.* **118**, 242 (1960). <https://doi.org/10.1103/PhysRev.118.242>
10. L.A. Rayburn, 14.4 MeV  $(n,2n)$  cross-sections. *Phys. Rev.* **122**, 168 (1961). <https://doi.org/10.1103/PhysRev.122.168>
11. J.T. Grissom, D.R. Koehler, W.L. Alford,  $^{141}\text{Nd}$  and its production in the  $(n,2n)$  reaction. *Phys. Rev.* **142**, 725 (1966). <https://doi.org/10.1103/PhysRev.142.725>

12. W. Dilg, H. Vonach, G. Winkler et al., Messung von  $(n,2n)$  wirkungs-querschnitten an schweren kernen. Nucl. Phys. A **118**, 9–16 (1968). [https://doi.org/10.1016/0375-9474\(68\)90182-6](https://doi.org/10.1016/0375-9474(68)90182-6)
13. P.R. Prasad, J.R. Rao, E. Kondaiah, Cross-sections for  $(n,2n)$ ,  $(n,\alpha)$  and  $(n,p)$  reactions in rare-earth isotopes at 14.2 MeV. Nucl. Phys. A **125**, 57–64 (1969). [https://doi.org/10.1016/0375-9474\(69\)90828-8](https://doi.org/10.1016/0375-9474(69)90828-8)
14. A. Bari, 14.8 MeV neutron activation cross-sections of rubidium, strontium, zirconium, niobium, and rare-earth nuclides. Dissertation Abstracts B (Sciences), **32**, 5091 (1972)
15. S.M. Qaim, Total  $(n,2n)$  cross-sections and isomeric cross-section ratios at 14.7 MeV in the region of rare earths. Nucl. Phys. A **224**, 319–330 (1974). [https://doi.org/10.1016/0375-9474\(74\)90690-3](https://doi.org/10.1016/0375-9474(74)90690-3)
16. S.L. Sothras, G.N. Salaita,  $(n,2n)$  cross-sections at 14.8 MeV on some closed shell nuclides. J. Inorg. Nucl. Chem. **40**, 585–587 (1978). [https://doi.org/10.1016/0022-1902\(78\)80371-6](https://doi.org/10.1016/0022-1902(78)80371-6)
17. S. Gmuca, I. Ribansky, Neutron activation cross-sections on Nd isotopes at 14.8 MeV. Acta Phys. Slovaca **33**, 9–23 (1983)
18. A.J. Do, J. Dresler, U. Garuska et al., The cross-sections of the  $(n,2n)$  reactions on  $^{134}\text{Ba}$ ,  $^{142}\text{Nd}$ ,  $^{150}\text{Nd}$  and  $^{144}\text{Sm}$ . J. Phys. G: Nucl. Phys. **10**, 91 (1984). <https://doi.org/10.1088/0305-4616/10/1/014>
19. J. Frehaut, A. Bertin, R. Bois et al., Status of  $(n, 2n)$  cross-section measurements at Bruyeres-le-Chatel. Report to the I.N.D.C., **1**, 399, 1980
20. N.L. Das, C.V.S. Rao, B.V.T. Rao et al., Pre-equilibrium effects in  $(n,2n)$  reactions at 14.2 MeV. Pramana **17**, 99–104 (1981). <https://doi.org/10.1007/BF02872041>
21. M.P. Menon, M.Y. Cuypers, 14.5 MeV neutron activation cross-section for some of the rare-earth nuclides and their relation to the nuclear shell structure. Phys. Rev. **156**, 1340 (1967). <https://doi.org/10.1103/PhysRev.156.1340>
22. Y. Kasugai, Y. Ikeda, and Y. Uno, Activation cross-section measurement for La, Ce, Pr, Nd, Gd, Dy and Er isotopes by 14 MeV neutrons. Technical report, 1997
23. M. Bormann, H.H. Bissem, E. Magiera et al., Total cross-sections and isomeric cross-section ratios for  $(n,2n)$  reactions in the energy region 12–18 MeV. Nucl. Phys. A **157**, 481–496 (1970). [https://doi.org/10.1016/0375-9474\(70\)90228-9](https://doi.org/10.1016/0375-9474(70)90228-9)
24. I. Kumabe, E. Kotake, F. Nagahama, Activation cross-sections for  $(n,2n)$  reaction on neodymium, samarium, gadolinium and ytterbium at 14.6 MeV. J. Nucl. Sci. Technol. **14**, 319–326 (1977). <https://doi.org/10.1080/18811248.1977.9730766>
25. Z.S. Pu, G.C. Wei, X.Z. Kong, Cross-section measurements for  $(n,2n)$  reactions on neodymium isotopes at the neutron energies of 13.5, 14.1 and 14.6 MeV. High Energy Phys. Nucl. **28**, 958–960 (2004). <https://doi.org/10.1023/B:JRNC.0000027073.70271.99>
26. J.H. Luo, L. An, L. Jiang et al., Cross-sections for D-T neutron interaction with neodymium isotopes. Radiat. Phys. Chem. **109**, 63–69 (2015). <https://doi.org/10.1016/j.radphyschem.2014.12.014>
27. Q. Wang, J.X. Zou, Z.H. Wang et al., Fission cross-section for the  $^{232}\text{Th}(n, f)^{138}\text{Cs}$  reaction induced by neutrons around 14 MeV. Eur. Phys. J. A **50**, 164 (2014). <https://doi.org/10.1140/epja/i2014-14164-0>
28. C.L. Lan, Y.J. Qiu, Q. Wang et al., Measurement of fission cross-section for  $^{232}\text{Th}(n,f)^{131}\text{Zr}$  ( $Z = 50,51,52,53$ ) reaction induced by neutrons around 14 MeV. Eur. Phys. J. A **53**, 131 (2017). <https://doi.org/10.1140/epja/i2017-12318-2>
29. C.L. Lan, B.L. Xie, K. Zhang et al., Measurement of  $^{232}\text{Th}(n,2n)^{231}\text{Th}$  reaction cross sections at neutron energies of 14.1 MeV and 14.8 MeV using neutron activation method. Nucl. Sci. Tech. **26**, 060501 (2015). <https://doi.org/10.13538/j.1001-8042/nst.26.060501>
30. C.L. Lan, M. Peng, Y. Zhang et al., Geant4 simulation of  $^{238}\text{U}(n, f)$  reaction induced by D-T neutron source. Nucl. Sci. Tech. **28**, 8 (2017). <https://doi.org/10.1007/s41365-016-0158-7>
31. Q. Wang, T. Liu, Y.J. Qiu et al., Measurement of the cross sections for  $^{238}\text{U}(n,\gamma)^{239}\text{U}$  reaction in the energy range of 14.1–14.8 MeV using neutron activation method. Radiat. Phys. Chem. **152**, 125–128 (2018). <https://doi.org/10.1016/j.radphyschem.2018.08.013>
32. K.H. Fang, S.W. Xu, C.L. Lan et al., Cross-section measurement for the reactions producing short-lived nuclei induced by neutrons around 14 MeV. Appl. Radiat. Isot. **66**, 1104–1107 (2008). <https://doi.org/10.1016/j.apradiso.2007.10.011>
33. V.E. Lewis, K.J. Zieba, A transfer standard for  $d + t$  neutron fluence and energy. Nucl. Instrum. Methods **174**, 141–144 (1980). [https://doi.org/10.1016/0029-554X\(80\)90422-X](https://doi.org/10.1016/0029-554X(80)90422-X)
34. K.A. Toukan, K. Debus, F. Käppler et al., Stellar neutron capture cross-sections of Nd, Pm, and Sm isotopes. Phys. Rev. C **51**, 1540 (1995). <https://doi.org/10.1103/PhysRevC.51.1540>
35. Q.Q. Cheng, Y.Z. Yuan, C.W. Ma et al., Gamma measurement based on CMOS sensor and ARM microcontroller. Nucl. Sci. Tech. **28**, 45–49 (2017). <https://doi.org/10.1007/s41365-017-0276-x>
36. R.B. Firestone, V.S. Shirley et al. *Table of Isotopes CD-ROM Edition*. Version 1.0, 1996
37. K.H. Fang, X.S. Xu, C.L. Lan et al., Cross-section measurement for  $\text{Ni}(n, x)^{58}(\text{m} + \text{g})\text{Co}$ ,  $\text{Ni}(n, x)^{60}\text{mCo}$ ,  $\text{Ni}(n, x)^{61}\text{Co}$  and  $\text{Ni}(n, x)^{62}\text{mCo}$  reactions induced by neutrons around 14 MeV. Chin. Phys. C **32**, 251–253 (2008). <https://doi.org/10.1088/1674-1137/32/4/002>
38. X.Z. Kong, Y.C. Wang, J.K. Yang, Cross-sections for  $(n,2n)$ ,  $(n,p)$  and  $(n,\alpha)$  reactions on rare-earth isotopes at 14.7 MeV. Appl. Radiat. Isot. **49**, 1529–1532 (1998). [https://doi.org/10.1016/S0969-8043\(98\)00018-9](https://doi.org/10.1016/S0969-8043(98)00018-9)
39. M.B. Chadwick, M. Herman, P. Obložinský et al., ENDF/B-VII.1: nuclear data for science and technology: cross-sections, covariances, fission product yields and decay data. Nucl. Data Sheets **112**, 2887–2996 (2011). <https://doi.org/10.1016/j.nds.2011.11.002>
40. Z.G. Ge, Z.X. Zhao, H.H. Xia et al., CENDL-3.1: the updated version of Chinese evaluated nuclear data library. J. Korean Phys. Soc. **59**, 1052–1056 (2011). <https://doi.org/10.3938/jkps.59.1052>
41. K. Shibata, O. Iwamoto, T. Nakagawa et al., JENDL-4.0: a new library for nuclear science and engineering. J. Nucl. Sci. Technol. **48**, 1–30 (2011). <https://doi.org/10.1080/18811248.2011.9711675>